Dalton Transactions

ROYAL SOCIETY OF CHEMISTRY

PAPER

View Article Online
View Journal | View Issue

Cite this: *Dalton Trans.*, 2026, **55**, 2080

Gallium phosphaketenes derived from bis(imino) acenaphthenes (bian): synthesis and reactivity towards a trityl radical and bian-gallylene

Alexandra A. Skatova,[a] Andrey A. Bazanov,[a] Evgeny V. Baranov,[a] Mikhail A. Kiskin,[b] Sergey Yu. Ketkov[a] and Igor L. Fedushkin*[a]

Phosphaketenes are important versatile reagents in organophosphorus chemistry. We herein report on the synthesis of novel mono- and bis-phosphaketenes based on redox-active acenaphthene-1,2-diimine ligands (bian) and their reactions with bian-gallylene and a trityl radical. The interaction of diiodide gallium (III) [(Ar^{BIG}-bian)GaI$_2$] (Ar^{BIG}-bian = 1,2-bis[(2,6-dibenzhydryl-4-methylphenyl)imino]acenaphthene) with two equivalents of sodium phosphaethynolate [Na(PCO)(diox)$_{0.5}$] gives the first paramagnetic phosphaketene [(Ar^{BIG}-bian)Ga(PCO)$_2$] (**1**). Reaction of **1** with gallylene [(Ar^{BIG}-bian)Ga] leads to phosphaketene [(Ar^{BIG}-bian)Ga(PCO)] (**2**). Gallium phosphaketene [(Ar^{BIG}-bian)Ga(Py)(PCO)] (**3**) is formed as a result of the interaction between diimine Ar^{BIG}-bian and excess gallium metal in the presence of gallium chloride in pyridine and a subsequent metathesis reaction with sodium phosphaethynolate. The addition of a trityl radical to **3** produces a sterically hindered alkyl complex [(Ar^{BIG}-bian)Ga(CPh$_3$)] (**4**). New compounds **1–4** have been characterized by ESR (**1**) and NMR (**2–4**) spectroscopy; their molecular structures have been established by single-crystal X-ray analysis. The electronic structures of **1–4** and reaction thermodynamics were studied by DFT calculations.

Received 13th October 2025,
Accepted 30th December 2025

DOI: 10.1039/d5dt02466h

rsc.li/dalton

Introduction

The chemistry of cyanate anions [OCN]$^-$ and their heavier analogs of the general formula [ChCPn]$^-$ (Ch = O–Te, Pn = N–As) is about two hundred years old and regularly experiences a renaissance since they are of exceptional interest both from a fundamental point of view (for example, the phenomenon of isomerism[1,2]) and for the preparation of practically important compounds.[3–6] The selenocyanate, [SeCN]$^-$, and tellurocyanate, [TeCN]$^-$, anions were the first to appear and are now fairly well studied.[3] A new stage in cyanate chemistry included the replacement of the nitrogen atom in cyanate anions [OCN]$^-$ by other pnictogens. These studies began in 1992 with the isolation of the phosphaethynolate anion [OCP]$^-$ as a component of [(DME)$_2$Li][OCP].[7] Although Shober and Spanutius synthesized anion [OCP]$^-$ in 1894,[8] the correct chemical formula was not determined at that time. Spectroscopic and computational studies have shown that the phosphaethynolate anion [OCP]$^-$ is an ambident nucleophile, and the oxygen ($^-$O–C≡P) or phosphorus (O=C=P$^-$) center can be the preferred site of reactivity in reactions of phosphaethynolate salts with various electrophiles, ammonium and imidazolium salts as well as in cycloaddition reactions.[9] Thus, the phosphaethynolate anion [OCP]$^-$ is a useful precursor for the synthesis of phosphorus-containing heterocycles and low valent phosphorus compounds.[4–6]

P-coordinated phosphaketenes of the general formula LnE–P=C=O (Ln = ligand, E = element of 13, 14 or 15 group) are unsaturated compounds, which show enhanced reactivity. While group 14 and group 15 element phosphaketenes have been well studied,[10–14] reports on group 13 element phosphaketenes,[15–22] especially gallium and indium,[19–22] are still very limited. The known group 13 element phosphaketenes include derivatives based on salen, bis(imino)acenaphthene, diimine and ketiminate ligands (Fig. 1). Note that aluminum prefers to bind to the oxygen atom of the [OCP]$^-$ anion, giving phosphaethynolate derivatives, while gallium and indium prefer to bind to the phosphorus atom of the PCO group, giving phosphaketenes, and in the case of boron, both options are possible.[21,22] The first representatives of bis-phosphaketenes, a new class of reactive group 13 metal-phosphorus compounds, have recently been synthesized.[22] Group 13 [OCP]$^-$-derivatives are promising candidates as precursors of molecules and materials with useful electronic properties, *e.g.* semiconducting materials for photovoltaic devices, solid state lasers, LEDs and optical waveguides.[23,24]

[a]*G. A. Razuvaev Institute of Organometallic Chemistry of the Russian Academy of Sciences, Tropinina Str. 49, Nizhny Novgorod, 603137, Russian Federation. E-mail: skatova@iomc.ras.ru*
[b]*N. S. Kurnakov Institute of General and Inorganic Chemistry, Russian Academy of Sciences, Leninsky Prosp. 31, Moscow 119991, Russian Federation*

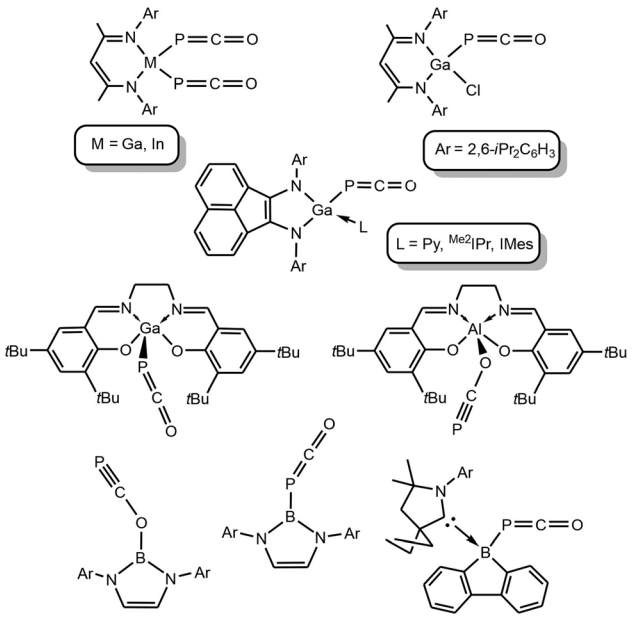

Fig. 1 Previously reported examples of group 13 phosphaethynolates and phosphaketenes.

Main group element phosphaketenes are a source of carbon monoxide due to the relatively weak P–CO bond and undergo decarbonylation reactions to afford gallium substituted diphosphenes or phosphinidenes containing a P═P bond[21] or to gallaphosphenes – unique compounds with a gallium–phosphorus double bond.[20–22] Gallaphosphenes were prepared by reactions of gallium phosphaketenes with gallylenes based on ketoiminate ligands.[20–22] In contrast to isoelectronic alkenes, gallaphosphenes have demonstrated very interesting reactivity, being able to react with carbon dioxide and heteroallenes through cycloaddition reactions[20,25] and with dihydrogen, carbonyl compounds, and compounds containing C(sp^3)–H and E–H bonds.[20,26]

Exploring the reactivity of bis(imino)acenaphthene derivatives of group 13 elements, including low-valent species, we have demonstrated their exceptional reactivity towards organic[27–34] and inorganic substrates, as well as small molecules, including SO_2[32] and carbon dioxide.[35,36] Very recently we have synthesized a stable gallylene of a new type – an open-shell compound with a redox-active ligand [(Ar^{BIG}-bian)Ga] (Ar^{BIG}-bian = 1,2-bis-[(2,6-dibenzhydryl-4-methylphenyl)imino] acenaphthene).[37] This work reports the synthesis of new gallium mono- and bis-phosphaketenes based on redox-active Ar^{BIG}-bian and their reactions with gallylene [(Ar^{BIG}-bian)Ga] and the trityl radical. Their ability to produce new gallaphosphenes is discussed.

Results and discussion

Synthesis and characterization of gallium bis-phosphaketene

The metathesis reaction of gallium diiodide [(Ar^{BIG}-bian)GaI_2] with two equivalents of sodium phosphaethynolate [Na(PCO)$(diox)_{0.5}$] in toluene solution leads to phosphaketene [(Ar^{BIG}-bian)Ga$(PCO)_2$] (**1**) as brown crystals with a yield of 56% (Scheme 1). Compound **1** is the first example of a paramagnetic phosphaketene and the second type of bis-phosphaketene after ketoiminate derivatives [$LM(PCO)_2$] (M = Ga, In; L = HC[C(Me)N(Ar)]$_2$; Ar = 2,6-$iPr_2C_6H_3$) prepared by S. Schulz and group.[22] The IR spectrum of **1** shows two strong peaks corresponding to the stretching vibrations of two PCO groups at 1909 and 1926 cm^{-1}, which lie in the region of the PCO frequencies observed for bis-phosphaketenes [$LM(PCO)_2$] (M = Ga, In; L = HC[C(Me)N(2,6-$iPr_2C_6H_3$)]$_2$) (1900–1940 cm^{-1}).[22] The calculated PCO vibrational frequencies of **1** (1915 and 1936 cm^{-1}) agree very well with the experiment. In contrast, the O-coordinated phosphaethynolate gallium derivatives[22] and starting Na(OCP)$(diox)_{0.5}$[38] show IR peaks in the region of 1730–1760 cm^{-1}.

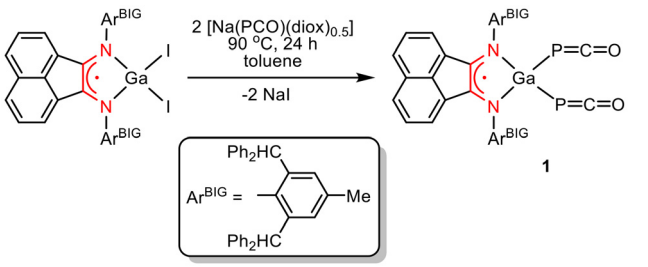

Scheme 1 Reaction of diiodide gallium(III) with sodium phosphaethynolate.

Compound **1** is paramagnetic. ESR spectroscopy unequivocally indicates the presence of the Ar^{BIG}-bian$^-$ radical anion in **1** (Fig. 2). The hyperfine structure of the ESR signal in toluene solution is caused by the coupling of an unpaired electron to the ^{69}Ga and ^{71}Ga isotopes, two non-equivalent nuclei ^{31}P, two equivalent ^{14}N nuclei of the diimine moiety, and two non-equivalent pairs of protons of the naphthalene backbone: g = 2.0051, a_i(2 × ^{14}N) = 0.454, a_i(2 × ^{1}H) = 0.090, a_i(2 × ^{1}H) = 0.120, a_i(^{69,71}Ga) = 1.511, a_i(^{31}P) = 0.716, a_i(^{31}P) = 0.717 mT.

The experimental hyperfine constants correlate well with the calculated isotropic Fermi contact couplings for most atoms (Table 1). Note that atomic spin densities on the Ga$(PCO)_2$ fragment (Table 1) are small despite the high hyperfine

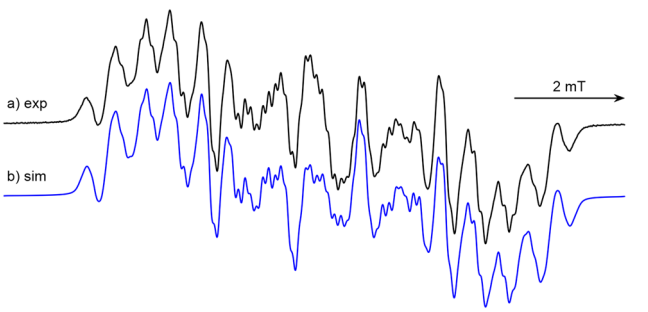

Fig. 2 Experimental (a) and simulated (b) ESR spectra of compound **1** (toluene, 340 K).

Table 1 Calculated[a] isotropic Fermi contact couplings A_i (mT) and Mulliken spin densities s (a.u.) on selected atoms of complex **1**. The atom numbering is given in Fig. 3(a)

Atom	A_i [b]	s
Ga	−2.493	−0.005
N(1)	0.497	0.230
N(2)	0.480	0.227
P(1)	0.676	0.003
P(2)	0.756	0.009
O(1)	−0.022	0.004
O(2)	−0.021	0.006
C(1)	0.574	0.199
C(2)	0.579	0.205
H(1)	−0.090	−0.002
H(2)	0.038	0.001
H(3)	−0.115	−0.003

[a] Calculations were performed at the B3LYP/6-31G(d) level of DFT. [b] Calculated for a model molecule bearing the 1,3-$^{i}Pr_2C_6H_3$ substituents instead of Ar^{BIG}, (dpp-bian)Ga(PCO)$_2$.

interaction constants. A similar situation was observed for gallylene [(Ar^{BIG}-bian)Ga].[37] The computed spin density distribution (Fig. 3b) shows the single electron to be delocalized over the bian core, which confirms its anion radical form.

Synthesis and reactivity of gallium mono-phosphaketenes

As has been previously shown, reactions of gallium phosphaketenes with ketiminate gallenes can lead to gallaphosphenes, rare compounds with a double gallium–phosphorus bond.[20–22] However, the reaction of **1** with recently prepared stable paramagnetic gallylene [(Ar^{BIG}-bian)Ga] in toluene does not lead to such a product,[22] but gives monophosphaketene [(Ar^{BIG}-bian)Ga(PCO)] (**2**) as brown crystals with a yield of 44% (Scheme 2). Computed thermodynamics nicely explains this behavior of complex **1**. The formation of gallaphosphene is endothermic and endergonic

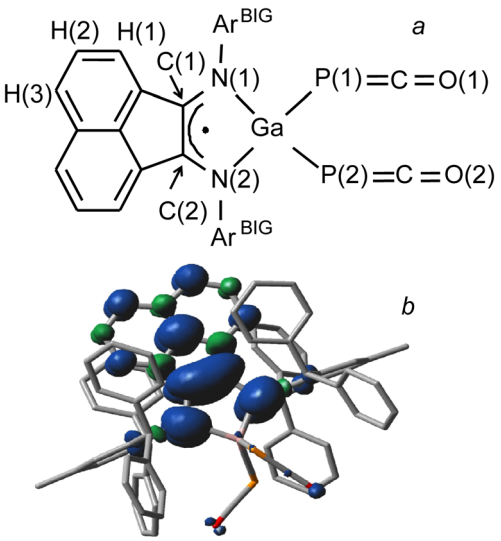

Fig. 3 Atom numbering (a) and spin density isosurface (b) (isovalue 0.01 a.u.) in molecule **1**.

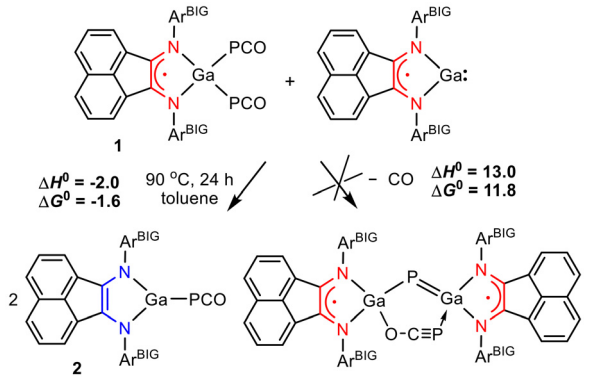

Scheme 2 Reaction of gallium bis-phosphaketene **1** with gallylene [(Ar^{BIG}-bian)Ga]. Calculated enthalpies and Gibbs free energies at 298 K (kcal mol^{-1}) are indicated.

($\Delta H^{\circ}_{298} = 13.0$ kcal mol^{-1}, $\Delta G^{\circ}_{298} = 11.8$ kcal mol^{-1}), which can be explained by the mutual repulsion of the very bulky Ar^{BIG} substituents in the two closely located Ar^{BIG}-bian ligands. In contrast, the formation of phosphaketene **2** is exothermic and exergonic ($\Delta H^{\circ}_{298} = -2.0$ kcal mol^{-1}, $\Delta G^{\circ}_{298} = -1.6$ kcal mol^{-1}). The symmetrization process is supported by the redox activity of the Ar^{BIG}-bian fragment, making possible the electron transfer from the metal atom to the ligand, which becomes formally dianionic.

For the preparative synthesis of gallium mono-phosphaketene from a halide precursor, the mono-chloride [(Ar^{BIG}-bian)Ga(Py)Cl] stabilized by the pyridine ligand was obtained by refluxing the diimine Ar^{BIG}-bian with excess gallium metal in the presence of gallium chloride in pyridine *in situ* (Scheme 3).

In contrast to dihalogen derivatives, the monochloride cannot be obtained from gallium chloride in the absence of a strong Lewis base. The addition of sodium phosphaethynolate to [(Ar^{BIG}-bian)Ga(Py)Cl] in DME solution and subsequent crystallization from the DME/Et_2O mixture give green crystals of mono-phosphaketene [(Ar^{BIG}-bian)Ga(Py)(PCO)] (**3**), containing the pyridine ligand coordinated to the gallium atom, unlike compound **2** (Scheme 3).

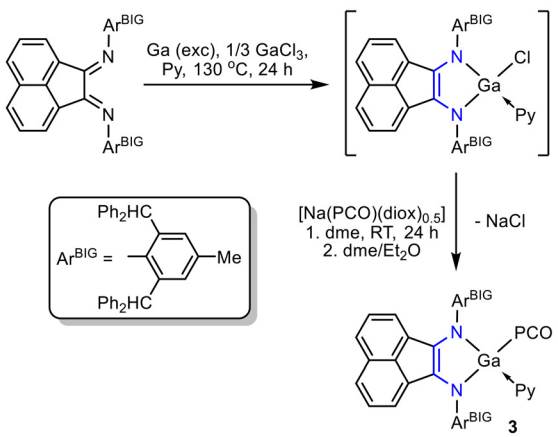

Scheme 3 Synthesis of gallium monophosphaketene **3**.

In the IR spectra, the PCO vibrations are responsible for the absorptions at 1975, 1960, and 1928 cm^{-1} (for **2**) and 1940, 1924, and 1912 cm^{-1} (for **3**), which are close to those observed for mono-phosphaketene [LGa(Cl)PCO] (1910 cm^{-1})[20] and the above-mentioned bis-phosphaketenes [LM(PCO)$_2$] (M = Ga, In; L = HC[C(Me)N(2,6-*i*Pr$_2$C$_6$H$_3$)]$_2$) (1900–1940 cm^{-1}),[22] as well as **1**.

Compounds **2** and **3** are diamagnetic due to the presence of the Ar^{BIG}-bian dianion and were characterized by NMR spectroscopy. The formation of the phosphaketenes is evidenced by singlet resonances in the $^{31}P\{^1H\}$ NMR spectra (δ = −368.8 (for **2**, see SI Fig. S2), −346.1 (for **3**, see SI Fig. S5) ppm). These values are in good agreement with previously reported bian-based [(dpp-bian)Ga(Py)(PCO)] ($^{31}P\{^1H\}$ NMR δ = −394.6)[21] and salen-supported ($^{31}P\{^1H\}$ NMR δ = −376.9 ppm)[19] gallium phosphaketenes. Unfortunately, the extremely low solubility of **2** and dynamic processes in the coordination sphere of **3** did not allow us to obtain informative ^{13}C NMR spectra of these complexes. The ^1H NMR spectra are given and interpreted in the SI (Fig. S3 and S4).

Although known phosphaketene [(dpp-bian)Ga(Py)(PCO)] reacts with gallium carbenoid [(Nacnac)Ga] to eliminate CO and yield base-stabilized gallaphosphene [(dpp-bian)Ga–P═Ga(Nacnac)(Py)] (Nacnac = HC[C(Me)*N*(2,6-*i*Pr$_2$C$_6$H$_3$)]$_2$),[22] compound **3** was found to be inert towards gallylene [(Ar^{BIG}-bian)Ga] probably due to steric hindrance. Moreover, DFT modeling of the dpp-bian analogue of the above-mentioned gallaphosphene, (dpp-bian)Ga–P═Ga(dpp-bian), demonstrates that this paramagnetic molecule has a low-lying vacant β-LUMO (−3.14 eV), suggesting high oxidative reactivity of the complex. For comparison, the β-LUMO of complex **1** and gallylene [(Ar^{BIG}-bian)Ga][37] lies at −2.75 and −2.58 eV, respectively.

Considering the ability of phosphaketenes to undergo decarbonylation with possible formation of gallaphosphenes containing a Ga═P bond, we added the trityl radical to **3** in THF solution. Recrystallization of the solid residue from the DME/hexane mixture gave brown crystals of the gallium alkyl derivative [(Ar^{BIG}-bian)Ga(CPh$_3$)] (**4**) with a yield of 24% (Scheme 4).

Thus, in this case the cleavage of the gallium–phosphorus bond took place. EPR spectroscopy monitoring of the reaction showed that several paramagnetic phosphorus-containing products (see SI Fig. S8) were formed during the reaction, which could not be isolated individually. According to DFT calculations, the formation of a gallylene adduct with phosphorus [(Ar^{BIG}-bian)Ga(P$_4$)] (**5**) as well as gallaphosphene [(Ar^{BIG}-bian)Ga═P–CPh$_3$] (**6**), containing the radical anion of the acenaphthene-1,2-diimine ligand (Scheme 5), is thermodynamically favorable (Table S3, see the SI). The corresponding reactions are accompanied by the elimination of carbon monoxide. Indeed this process was observed during the interaction of **3** with Ph$_3$C$^{\bullet}$.

The ^1H NMR spectrum of compound **4** corresponds to a symmetric geometry of the gallium center in solution, which is evident from the presence of only one signal (δ = 5.97 ppm) of the four methine protons C*H*Ph$_2$ of the benzhydryl substituents (see SI Fig. S6). The ^{13}C NMR spectrum of **4** shows a signal at δ 68.8 ppm corresponding to the CPh$_3$ group (Fig. S7, see the SI). Note that compound **4** can be obtained by the direct reaction of gallylene [(Ar^{BIG}-bian)Ga] with a trityl radical (Scheme 4). The reaction proceeds at the rate of mixing of the reagents. The ^1H NMR spectrum of the reaction mixture in THF-d$_8$ solution demonstrated complete conversion of the reagents to product **4** (see SI Fig. S9). According to ESR spectroscopic monitoring, the gallium–carbon bond in compound **4** does not dissociate in solution even when heated. DFT predicts the Ga–C bond dissociation enthalpy in the THF solution to be only 8.9 kcal mol^{-1}, which seems to be an underestimated value. This discrepancy with the experimental stability of complex **4** can be explained by high energies of structural transformations of the (Ar^{BIG}-bian)Ga and CPh$_3$ fragments on moving from **4** to free molecules.

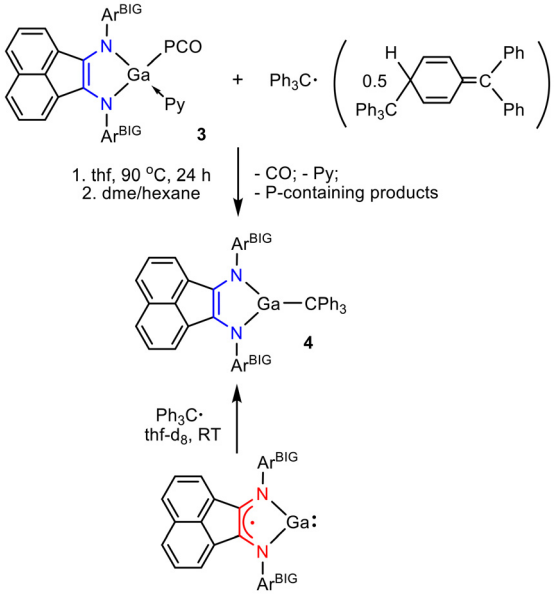

Scheme 4 Reactions of gallium phosphaketene **3** and gallylene with the trityl radical.

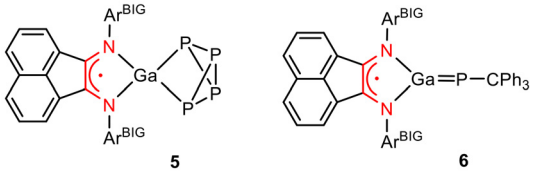

Scheme 5 Possible paramagnetic byproducts formed in the reaction of complex **3** with the trityl radical.

Molecular structures of compounds 1–4

The molecular structures of compounds **1–4** were determined using single-crystal X-ray diffraction analysis and are depicted in Fig. 4–7. For the crystallographic data, structure refinement details and selected bond lengths and angles, see the SI (Tables S1 and S2).

Compounds **1–4** represent mononuclear four- (**1**, **3**) and three- (**2**, **4**) coordinated gallium complexes. In complex **1**, the

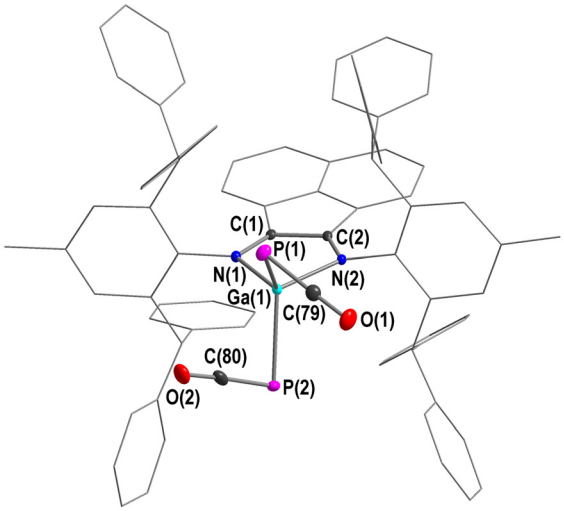

Fig. 4 Molecular structure of **1** with thermal ellipsoids at 30% probability. H atoms are omitted for clarity.

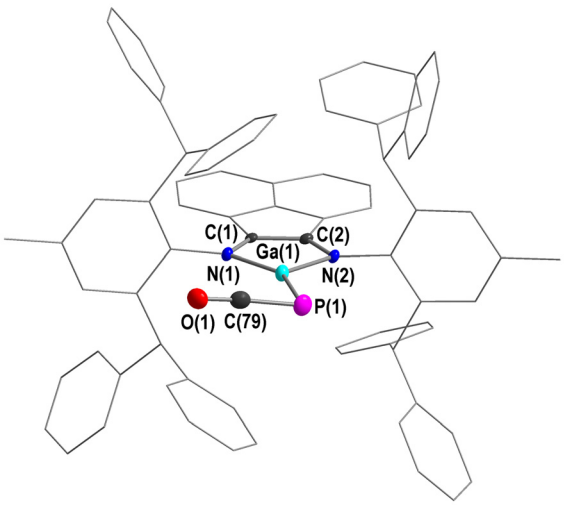

Fig. 5 Molecular structure of **2** with thermal ellipsoids at 30% probability. H atoms are omitted for clarity.

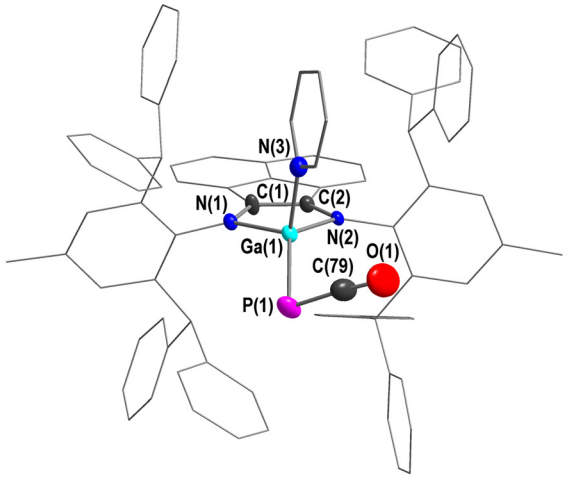

Fig. 6 Molecular structure of **3** with thermal ellipsoids at 30% probability. H atoms are omitted for clarity.

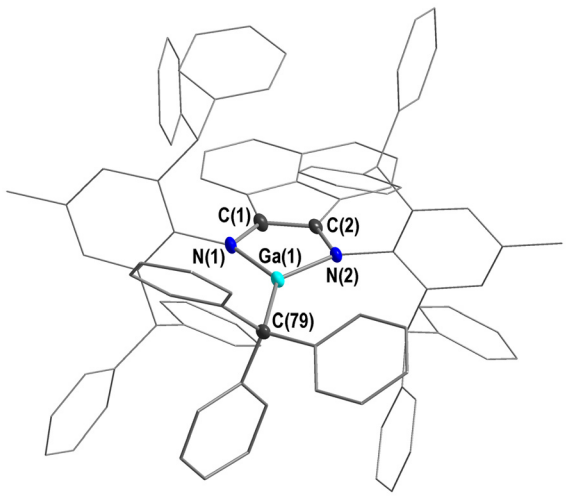

Fig. 7 Molecular structure of **4** with thermal ellipsoids at 30% probability. H atoms are omitted for clarity.

Ar^{BIG}-bian ligand is a radical anion: 1.339(2) and 1.342(2) Å for the N–C and 1.433(2) Å for the C–C bond lengths. In complexes **2–4**, the bond lengths of the diimine fragment correspond to the dianionic form of the ligand: N–C 1.372(4)–1.403(4) Å and C–C 1.372(6)–1.393(4) Å. The gallium atoms in **1** and **3** adopt a distorted tetrahedral geometry. In all compounds, gallium atoms are bonded to two nitrogen atoms of the bian-ligand, as well as to phosphorus atoms in **1–3**, which confirms the corresponding type of bonding with PCO groups. The bond angles about the PCO moiety are typical of compounds of this class, with approximately linear O–C–P (172.6(5)–177.5(2)°) and Ga–P–C angles ranging from 83.26(8) to 91.50(16)°. The distances between the atoms in the [Ga]–P═C═O fragments of **1–3** (P–$C_{av.}$ 1.633(1), C–$O_{av.}$ 1.168(2) Å) correspond to double bonds and are close to those in the gallium phosphaketenes [(dpp-bian)GaPy(PCO)][21] (P–C 1.636(3) Å, C–O 1.165(3) Å) and [salen(*t*Bu)Ga(PCO)][19] (P–C 1.625(4), C–O 1.189(4) Å). For comparison, in the aluminium phosphaethynolate [salen(*t*Bu)Al(PCO)(thf)],[19] the [Al]–O–C≡P group bond lengths are as follows: O–C 1.228(5), C–P 1.587(5) Å.

In complex **2**, the Ga–PCO fragment almost lies in the plane of the metallacycle (Fig. 5). In compound **3**, the dihedral angle between the planes of the metallacycle GaNNCC and the GaPCO is 118°. The coordination environment of the gallium atom in alkyl complex **4** (Fig. 7) is nearly triangle like in **2**. The sum of the angles around the Ga atom in **2** and **4** is 360° and 359°, respectively. The analogous sum of angles in **3** is smaller and equals 336°. The phenyl rings of the Ph_3C group are arranged in a propeller shape and are caught between the phenyls of the benzhydryl substituents of the Ar^{BIG}-bian

ligand. The Ga–C(trityl) distance in **4** (1.991(4) Å) is longer than the Ga–C (1.9330(19) Å) bond length in the alkyl gallium complex [(Ar^{BIG}-bian)Ga*n*Pr][38] due to the large steric bulk of the Ph_3C group.

Electronic structures of compounds 1–4

Complexes **1–4** obtained in this work contain the (Ar^{BIG}-bian)Ga fragment bearing various additional ligands (PCO, Py, and CPh_3). To study their influence on the electronic structures, DFT analysis of the frontier MOs was carried out at the B3LYP/6-31G(d) level of DFT,[40] which demonstrated good performance in our previous studies of the bian complexes.[35,37,39] The optimized geometries of molecules **1–4** agree well with the X-ray data (Tables S2, S3, see the SI). The ground electronic state of complex **1** is a doublet, like in gallylene (Ar^{BIG}-bian)Ga.[37] The single electron occupies the α-HOMO (−4.63 eV), which is delocalized mainly along the CNNC fragment of Ar^{BIG}-bian (Fig. 8). This is confirmed by the spin density distribution (Fig. 3). The corresponding vacant β-LUMO lies at −2.78 eV. The addition of the two PCO groups to the (Ar^{BIG}-bian)Ga gallylene[38] decreases the α-HOMO and β-LUMO energies by 0.30 and 0.20 eV, respectively. This decrease is associated with the stronger electron withdrawing ability of the Ga^{3+} cation in **1** compared to Ga^{+} in the gallylene. Indeed the Ar^{BIG}-bian fragment charges in **1** and (Ar^{BIG}-bian)Ga, computed by the frames of Bader's quantum theory of atoms in molecules (QT AIM),[41,42] are −0.495 *e* and −0.625 *e*, respectively.

The HOMO shapes of complexes **2–4** resemble that of α-HOMO in **1** (Fig. 8). However, for compounds **2** and **4** with the triangular coordination environment of the metal atom, an increased Ga contribution to the HOMO is observed. The **2–4** HOMOs lie higher in energy than the α-HOMO of **1**, which is a result of a more negative charge of [Ar^{BIG}-bian]$^{2-}$ in **2–4** compared to [Ar^{BIG}-bian]$^{-}$ in **1**. The **2** and **4** HOMO energies are close (Fig. 8), whereas the addition of the donor Py ligand to molecule **2** increases the HOMO energy by 0.42 eV, which agrees with the more negative Ar^{BIG}-bian fragment in **3**.

Unlike the HOMO, the LUMO distribution in complexes **2–4** varies greatly. The LUMO of complex **2** is delocalized predominantly along the GaPCO fragment. In molecule **3**, the LUMO is a pyridine orbital, whereas in complex **4**, the LUMO is delocalized over the acenaphthene moiety of the Ar^{BIG}-bian ligand. The **4** LUMO shape resembles that of α-LUMO in complex **1** (Fig. 8). However, the replacement of two PCO groups with CPh_3 leads to a significant shift of the LUMO towards less negative energies.

The frontier orbital energies in closed-shell systems **2–4** increase in the row E^{HOMO}(**2**) < E^{HOMO}(**4**) < E^{HOMO}(**3**) and E^{LUMO}(**3**) < E^{LUMO}(**2**) < E^{LUMO}(**4**). As a result, complex **3** possesses the lowest HOMO–LUMO energy gap of 1.81 eV (Fig. 8). The addition of a Py fragment to the Ga atom of **2** causes surprisingly strong changes in the electronic structure. The HOMO–LUMO gap decreases by 0.55 eV on moving from **2** to **3** (Fig. 8). The donor Py ligand shifts electron density (0.149 *e* as predicted by QT AIM analysis) towards the (Ar^{BIG}-bian)Ga(PCO) fragment. However, the Ga atom unexpectedly becomes more positively charged (1.322 *e* in **2** *vs.* 1.506 *e* in **3**). On the other hand, the (Ar^{BIG}-bian) and PCO ligands in **3** become more negative by 0.212 *e* and 0.119 *e*, respectively, as compared to **2**. Therefore, the addition of donor ligands to complex **2** can be used to modify the frontier MO energies and charge distribution.

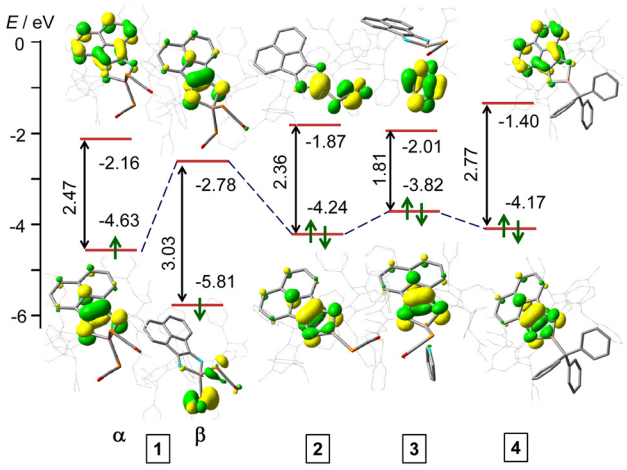

Fig. 8 Frontier MO diagrams of complexes **1–4**. MO energies and HOMO–LUMO energy gaps (eV) are indicated.

Conclusions

In summary, we have expanded the range of rare gallium phosphaketenes to include mono- and bis-phosphaketenes supported by a sterically hindered (bis)iminoacenaphthene diimine ligand Ar^{BIG}-bian. In these compounds, the redox-active diimine ligand is either a dianion or a radical anion. The paramagnetic phosphaketene was obtained for the first time. The addition of paramagnetic gallium(I) carbenoid [(Ar^{BIG}-bian)Ga] to the obtained bisphosphaketene [(Ar^{BIG}-bian)Ga(PCO)$_2$], containing the diimine radical anion, leads to the diamagnetic monophosphaketene [(Ar^{BIG}-bian)Ga(PCO)] bearing the dianionic Ar^{BIG}-bian fragment. The symmetrization process is accompanied by the metal–ligand electron transfer. The addition of the trityl radical to phosphaketene [(Ar^{BIG}-bian)Ga(Py)(PCO)] or to gallylene leads to the formation of a sterically hindered alkyl gallium complex [(Ar^{BIG}-bian)Ga(CPh_3)]. The phenyl rings of the Ph_3C group are located between the phenyls of the benzhydryl substituents of the Ar^{BIG}-bian ligand, which stabilizes this compound. DFT calculations demonstrate that the addition of PCO, Py or CPh_3 groups to the Ga atom of [(Ar^{BIG}-bian)Ga] results in significant changes in the orbital structure as well as in the charge distribution. This can strongly affect the reactivity of the compounds. In the future, the reactivity of the obtained complexes towards small molecules and unsaturated compounds will be studied by our group.

Author contributions

A. A. S. conceptualization, supervision, project administration, writing – original draft, and writing – review & editing; A. A. B. formal analysis, data curation, investigation, and writing of the SI; E. V. B. formal analysis and investigation; M. A. K. formal analysis and investigation; S. Y. K. formal analysis, methodology, and writing – original draft; I. L. F. conceptualization, supervision, and writing – review & editing.

Conflicts of interest

There are no conflicts to declare.

Data availability

The data that support the findings of this study are available within the article and its supplementary information (SI). Supplementary information: experimental section, spectral characteristics (ESR and NMR spectra), crystal data and structural refinement details. See DOI: https://doi.org/10.1039/d5dt02466h.

CCDC 2479698–2479701 contain the supplementary crystallographic data for this paper.[43a–d]

Acknowledgements

This work was supported by the Russian Science Foundation (grant 25-13-00268 – the experimental part, project 23-13-00139 – DFT calculations). This work was carried out using the equipment of the centers for collective use "Analytical Center of the IOMC RAS" and single crystal X-ray diffraction investigations (of samples **3** and **4**) were performed using the equipment of the "JRC PMR IGIC RAS".

References

1 F. Kurzer, Fulminic Acid in the History of Organic Chemistry, *J. Chem. Educ.*, 2000, **77**, 851–857.
2 F. Kurzer, The Life and Work of Edward Charles Howard FRS, *Ann. Sci.*, 1999, **56**, 113–141.
3 S. Hohloch and F. Tambornino, Historical and Recent Developments in the Chemistry of Cyanate Congeners, *Inorg. Chem.*, 2025, **64**, 12900–12917.
4 L. Weber, 2-Phospha- and 2-Arsaethynolates – Versatile Building Blocks in Modern Synthetic Chemistry, *Eur. J. Inorg. Chem.*, 2018, 2175–2227.
5 J. M. Goicoechea and H. Grützmacher, The Chemistry of the 2-Phosphaethynolate Anion, *Angew. Chem., Int. Ed.*, 2018, **57**, 16968–16994.
6 X. Chen, S. Alidori, F. Frank Puschmann, G. Santiso-Quinones, Z. Benkö, Z. Li, G. Becker, H.-F. Grützmacher and H. Grützmacher, Sodium Phosphaethynolate as a Building Block for Heterocycles, *Angew. Chem., Int. Ed.*, 2014, **53**, 1641–1645.
7 G. Becker, W. Schwarz, N. Seidler and M. Westerhausen, Acyl- und Alkylidenphosphane. XXXIII. Lithoxy-methylidenphosphan DME und -methylidinphosphan 2 DME – Synthese und Struktur, *Z. Anorg. Allg. Chem.*, 1992, **612**, 72–82.
8 W. B. Shober and F. W. Spanutius, On Phospho-Hydrocyanic Acid, *Am. Chem. J.*, 1894, (16), 229–233.
9 D. Heift, Z. Benkő and H. Grützmacher, Is the phosphaethynolate anion, $(OCP)^-$, an ambident nucleophile? A spectroscopic and computational study, *Dalton Trans.*, 2014, **43**, 5920–5928.
10 S. Yao, Y. Xiong, T. Szilvási, H. Grützmacher and M. Driess, From a Phosphaketenyl-Functionalized Germylene to 1,3-Digerma-2,4-diphosphacyclobutadiene, *Angew. Chem., Int. Ed.*, 2016, **55**, 4781–4785.
11 Y. Xiong, S. Yao, T. Szilvási, E. Ballestero-Martínez, H. Grützmacher and M. Driess, Unexpected Photodegradation of a Phosphaketenyl-Substituted Germyliumylidene Borate Complex, *Angew. Chem., Int. Ed.*, 2017, **56**, 4333–4336.
12 Z. Li, X. Chen, M. Bergeler, M. Reiher, C. Y. Su and H. Grützmacher, A stable phosphanyl phosphaketene and its reactivity, *Dalton Trans.*, 2015, **44**, 6431–6438.
13 L. Liu, D. A. Ruiz, D. Munz and G. Bertrand, A Singlet Phosphinidene Stable at Room Temperature, *Chem*, 2016, **1**, 147–153.
14 M. M. Hansmann, D. A. Ruiz, L. Liu, R. Jazzar and G. Bertrand, (Phosphanyl)phosphaketenes as building blocks for novel phosphorus heterocycles, *Chem. Sci.*, 2017, **8**, 3720–3725.
15 D. W. N. Wilson, M. P. Franco, W. K. Myers, J. E. McGrady and J. M. Goicoechea, Base induced isomerisation of a phosphaethynolato-borane: mechanistic insights into boryl migration and decarbonylation to afford a triplet phosphinidene, *Chem. Sci.*, 2020, **11**, 862–869.
16 W. Yang, K. E. Krantz, D. A. Dickie, A. Molino, D. J. D. Wilson and R. J. Gilliard, Crystalline BP-Doped Phenanthryne via Photolysis of The Elusive Boraphosphaketene, *Angew. Chem., Int. Ed.*, 2020, **59**, 3971–3975.
17 W. Yang, K. E. Krantz, D. A. Dickie, A. Molino, D. J. D. Wilson and R. J. Gilliard Jr., Crystalline BP-Doped Phenanthryne via Photolysis of The Elusive Boraphosphaketene, *Angew. Chem., Int. Ed.*, 2020, **58**, 3971–3975.
18 S. Hagspiel, F. Fantuzzi, R. D. Dewhurst, A. Gärtner, F. Lindl, A. Lamprecht and H. Braunschweig, Adducts of the Parent Boraphosphaketene H_2BPCO and their Decarbonylative Insertion Chemistry, *Angew. Chem., Int. Ed.*, 2021, **60**, 13666–13670.
19 Y. Mei, J. E. Borger, D. J. Wu and H. Grützmacher, Salen supported Al–O–C≡P and Ga–P=C=O complexes, *Dalton Trans.*, 2019, **48**, 4370–4374.
20 M. K. Sharma, C. Wölper, G. Haberhauer and S. Schulz, Multi-Talented Gallaphosphene for Ga–P–Ga Heteroallyl

Cation Generation, CO_2 Storage, and C(sp^3)–H Bond Activation, *Angew. Chem., Int. Ed.*, 2021, **60**, 6784–6790.
21 D. Wilson, W. Myers and J. M. Goicoechea, Synthesis and decarbonylation chemistry of gallium phosphaketenes, *Dalton Trans.*, 2020, **49**, 15249–15255.
22 M. K. Sharma, P. Dhawan, C. Helling, C. Wölper and S. Schulz, Bis-Phosphaketenes $LM(PCO)_2$ (M = Ga, In): A New Class of Reactive Group 13 Metal-Phosphorus Compounds, *Chem. – Eur. J.*, 2022, **28**, e202200444.
23 F. Dimroth, High-efficiency solar cells from III-V compound semiconductors, *Phys. Status Solidi C*, 2006, **3**, 373–379.
24 M. R. Krames, O. B. Shchekin, R. Mueller-Mach, G. O. Mueller, L. Zhou, G. Harbers and M. G. Craford, Status and Future of High-Power Light-Emitting Diodes for Solid-State Lighting, *J. Disp. Technol.*, 2007, **3**, 160–175.
25 M. K. Sharma, K. Wölper, G. Haberhauer and S. Schulz, Reversible and Irreversible [2 + 2] Cycloaddition Reactions of Heteroallenes to a Gallaphosphene, *Angew. Chem., Int. Ed.*, 2021, **60**, 21784–21788.
26 M. K. Sharma, K. Wölper and S. Schulz, Selective 1,2 addition of polar X–H bonds to the Ga–P double bond of gallaphosphene L(Cl) GaPGaL, *Dalton Trans.*, 2022, **51**, 1612–1616.
27 I. L. Fedushkin, A. S. Nikipelov and K. A. Lyssenko, Reversible Addition of Alkynes to Gallium Complex of Chelating Diamide Ligand, *J. Am. Chem. Soc.*, 2010, **132**, 7874–7875.
28 I. L. Fedushkin, A. S. Nikipelov, A. G. Morozov, A. A. Skatova, A. V. Cherkasov and G. A. Abakumov, Addition of Alkynes to a Gallium Bis-Amido Complex: Imitation of Transition-Metal-Based Catalytic Systems, *Chem. – Eur. J.*, 2012, **18**, 255–266.
29 W. Zhang, V. A. Dodonov, W. Chen, Y. Zhao, A. A. Skatova, I. L. Fedushkin, P. W. Roesky, B. Wu and X.-J. Yang, Cycloaddition versus Cleavage of the C = S Bond of Isothiocyanates Promoted by Digallane Compounds with Noninnocent α-Diimine Ligands, *Chem. – Eur. J.*, 2018, **24**, 14994–15002.
30 V. A. Dodonov, W. Chen, Y. Zhao, A. A. Skatova, P. W. Roesky, B. Wu, X.-J. Yang and I. L. Fedushkin, Gallium "Shears" for C = N and C = O Bonds of Isocyanates, *Chem. – Eur. J.*, 2019, **25**, 8259–8267.
31 I. L. Fedushkin, V. A. Dodonov, A. A. Skatova, V. G. Sokolov, A. V. Piskunov and G. K. Fukin, Redox-Active Ligand Assisted Two-Electron Oxidative Addition to Gallium(II), *Chem. – Eur. J.*, 2018, **24**, 1877–1889.
32 I. L. Fedushkin, A. A. Skatova, V. A. Dodonov, X.-J. Yang, V. A. Chudakova, A. V. Piskunov, S. Demeshko and E. V. Baranov, Ligand "Brackets" for Ga-Ga Bond, *Inorg. Chem.*, 2016, **55**, 9047–9056.
33 V. A. Dodonov, W. Chen, L. Liu, V. G. Sokolov, E. V. Baranov, A. A. Skatova, Y. Zhao, B. Wu, X.-J. Yang and I. L. Fedushkin, Reactions of Iso(thio)cyanates with Dialanes: Cycloaddition, Reductive Coupling, or Cleavage of C = S/C = O Bond, *Inorg. Chem.*, 2021, **60**, 14602–14612.
34 T. S. Koptseva, A. A. Skatova, M. V. Moskalev, R. V. Rumyantcev and I. L. Fedushkin, Hydro-coupling of Isocyanates Promoted by Acenaphthenediimine Aluminum Hydrides, *Dalton Trans.*, 2024, **53**, 17308–17312.
35 T. S. Koptseva, V. G. Sokolov, S. Yu. Ketkov, E. A. Rychagova, A. V. Cherkasov, A. A. Skatova and I. L. Fedushkin, Reversible Addition of Carbon Dioxide to Main Group Metal Complexes at Temperatures about 0 °C, *Chem. – Eur. J.*, 2021, **27**, 5745–5753.
36 V. A. Dodonov, O. A. Kushnerova, E. V. Baranov, A. S. Novikov and I. L. Fedushkin, Activation and modification of carbon dioxide by redox-active low-valent gallium species, *Dalton Trans.*, 2021, **50**(25), 8899–8906.
37 N. L. Bazyakina, A. A. Skatova, M. V. Moskalev, E. V. Baranov, T. S. Koptseva, S. Y. Ketkov, X.-J. Yang and I. L. Fedushkin, Synthesis and Reactivity of Stable Open-Shell Gallylene, *Inorg. Chem.*, 2025, **64**, 4892–4901.
38 F. F. Puschmann, D. Stein, D. Heift, C. Hendriksen, Z. A. Gál, H.-F. Grützmacher and H. Grützmacher, Phosphination of Carbon Monoxide: A Simple Synthesis of Sodium Phosphaethynolate (NaOCP), *Angew. Chem., Int. Ed.*, 2011, **50**, 8420–8423.
39 I. L. Fedushkin, A. N. Lukoyanov, S. Y. Ketkov, M. Hummert and H. Schumann, [(dpp-bian)Ga-Ga(dpp-bian)] and [(dpp-bian)Zn-Ga(dpp-bian)]: synthesis, molecular structures, and DFT studies of these novel bimetallic molecular compounds, *Chem. – Eur. J.*, 2007, **13**, 7050–7056.
40 M. J. Frisch, et al., *DFT calculations were carried out using the Gaussian 09 program suit. Gaussian 09, Revision D.01*, Gaussian, Inc., Wallingford CT, 2013. See the SI for a detailed description.
41 R. F. W. Bader, *Atoms in Molecules: A Quantum Theory*, Oxford University Press, Oxford, 1990.
42 F. Cortés-Guzmán and R. F. W. Bader, Complementarity of QTAIM and MO theory in the study of bonding in donor–acceptor complexes, *Coord. Chem. Rev.*, 2005, **249**, 633–662.
43 (*a*) CCDC 2479698: Experimental Crystal Structure Determination, 2026, DOI: 10.5517/ccdc.csd.cc2p7b8k; (*b*) CCDC 2479699: Experimental Crystal Structure Determination, 2026, DOI: 10.5517/ccdc.csd.cc2p7b9l; (*c*) CCDC 2479700: Experimental Crystal Structure Determination, 2026, DOI: 10.5517/ccdc.csd.cc2p7bbm; (*d*) CCDC 2479701: Experimental Crystal Structure Determination, 2026, DOI: 10.5517/ccdc.csd.cc2p7bcn.